Petroleum Science 20 (2023) 1142–1154

Contents lists available at ScienceDirect

Petroleum Science

journal homepage: www.keaipublishing.com/en/journals/petroleum-science

Original Paper

Few-shot working condition recognition of a sucker-rod pumping system based on a 4-dimensional time-frequency signature and meta-learning convolutional shrinkage neural network

Yun-Peng He [a, b, c, d], Chuan-Zhi Zang [e], Peng Zeng [a, b, c, *], Ming-Xin Wang [a, b, c, f], Qing-Wei Dong [a, b, c, d], Guang-Xi Wan [a, b, c, d], Xiao-Ting Dong [a, b, c, d]

[a] State Key Laboratory of Robotics, Shenyang Institute of Automation, Chinese Academy of Sciences, Shenyang, Liaoning 110016, China
[b] Key Laboratory of Networked Control Systems, Chinese Academy of Sciences, Shenyang, Liaoning 110016, China
[c] Institutes for Robotics and Intelligent Manufacturing, Chinese Academy of Sciences, Shenyang, Liaoning 110169, China
[d] University of Chinese Academy of Sciences, Beijing, 100049, China
[e] Shenyang University of Technology, Shenyang, Liaoning 110870, China
[f] School of Automation and Electrical Engineering, Shenyang Ligong University, Shenyang, Liaoning 110159, China

ARTICLE INFO

Article history:
Received 5 January 2022
Received in revised form
16 February 2023
Accepted 16 February 2023
Available online 24 February 2023

Edited by: Xiu-Qiu Peng

Keywords:
Few-shot learning
Indicator diagram
Meta-learning
Soft thresholding
Sucker-rod pumping system
Time–frequency signature
Working condition recognition

ABSTRACT

The accurate and intelligent identification of the working conditions of a sucker-rod pumping system is necessary. As onshore oil extraction gradually enters its mid-to late-stage, the cost required to train a deep learning working condition recognition model for pumping wells by obtaining enough new working condition samples is expensive. For the few-shot problem and large calculation issues of new working conditions of oil wells, a working condition recognition method for pumping unit wells based on a 4-dimensional time-frequency signature (4D-TFS) and meta-learning convolutional shrinkage neural network (ML-CSNN) is proposed. First, the measured pumping unit well workup data are converted into 4D-TFS data, and the initial feature extraction task is performed while compressing the data. Subsequently, a convolutional shrinkage neural network (CSNN) with a specific structure that can ablate low-frequency features is designed to extract working conditions features. Finally, a meta-learning fine-tuning framework for learning the network parameters that are susceptible to task changes is merged into the CSNN to solve the few-shot issue. The results of the experiments demonstrate that the trained ML-CSNN has good recognition accuracy and generalization ability for few-shot working condition recognition. More specifically, in the case of lower computational complexity, only few-shot samples are needed to fine-tune the network parameters, and the model can be quickly adapted to new classes of well conditions.

1. Introduction

Sucker-rod pumping systems have the merits of low comprehensive costs, simple equipment and convenient operation and have been widely used in mechanical oil recovery. Rod pumping equipment needs to be extended underground for thousands of meters during the working process, the working conditions are very complicated, and the working environment is also very harsh, causing a high failure rate, which seriously affects the production efficiency of oil fields (Li et al., 2018). Once oil wells fail to produce oil normally, there will be various consequences that can lead to production shutdown, causing very large economic losses. Therefore, it is essential to quickly and accurately identify the working conditions of a pumping well with a sucker rod (Lv et al., 2021a).

Currently, the mainstream working condition identification method determines the working conditions of pumping wells by identifying the indicator diagram (Han et al., 2021; Lv et al., 2020; Zheng et al., 2020). In the traditional method, the staff identifies faults through indicator diagram analysis based on their own experience. Since this method is simple and convenient to operate

* Corresponding author. State Key Laboratory of Robotics, Shenyang Institute of Automation, Chinese Academy of Sciences, Shenyang, Liaoning, 110016, China.
E-mail address: zp@sia.cn (P. Zeng).

https://doi.org/10.1016/j.petsci.2023.02.017

and can identify most faults, it has not been eliminated thus far. However, this method has poor accuracy and low efficiency and cannot satisfy the requirements of modern oilfield production.

In recent years, intelligent diagnosis technologies, such as support vector machines (SVMs) (Lv et al., 2021b), designated component analysis theory (Li et al., 2013a), spectral clustering (Li et al., 2015), hidden Markov models (Zheng and Gao, 2017) and radial basis function (RBF) neural networks (Zhou et al., 2019), have been developed rapidly, especially deep learning-based oilfield working condition diagnosis methods (Peng, 2019; Zhang et al., 2022), which has greatly improved the accuracy and efficiency of well condition identification. For instance, (Li et al., 2013b) employed a moment-curve method to obtain the features of indicator diagrams and used a modified SVM for work condition identification. (Zheng and Gao, 2017) used the center-of-gravity decomposition algorithm to obtain the geometric features of an indicator diagram and a Markov model for work condition recognition. (Wang et al., 2019) suggested a 14-layer convolutional neural network (CNN) diagnostic model based on big data and deep learning for the identification of the working conditions of rod pumping wells. (Cheng et al., 2020) proposed a strategy to improve the accuracy and efficiency of fault diagnosis by using a combination of CNNs and SVMs with error-correcting output code models for work condition identification.

Existing intelligent diagnosis methods mainly obtain working conditions by manually preselecting the geometric features of an indicator diagram, and an intelligent algorithm classifies them according to the corresponding features of the indicator diagram (Li et al., 2015). Although the various intelligent diagnosis methods mentioned above have achieved certain results, two problems still exist. (**i**), different from the general image recognition, an oilfield indicator diagram has the characteristics of simple image and few feature points. It is directly input into the algorithm as a two-dimensional image, which causes low feature utilization and large data calculation amount to a certain extent. (**ii**), it is impossible to obtain enough work condition samples for model training. Specifically, most of the onshore oil fields have entered the middle or even late stage of exploitation. As the working time of an oil well grows, new working conditions will be added, oil well failure will occur increasingly frequently, and serious safety accidents can occur when oil wells are in a state of failure for a long time.

To address the first problem, researchers have developed work condition recognition strategies that use feature extraction methods. High feature dimensionality (Han et al., 2021), center-of-gravity decomposition (Zheng and Gao, 2017), curve moment (Li et al., 2013b), Fourier descriptor (Zhou et al., 2019), wavelet transform (Wu et al., 2011) and statistical feature (Zheng et al., 2019) methods are often applied to extract features of dynamometer cards, but there are shortcomings, such as the computational complexity, high feature dimensions, and sensitivity to noise (Han et al., 2021). With the application of CNNs in the field of pattern recognition, CNN is used to extract features directly from indicator diagrams. For illustration, (Sharaf, 2018) used three improved artificial neural networks, VGG16, ResNet34 and ResNet50, for well working condition recognition based on the pump card shape and confirmed that the highest accuracy was achieved at the last layer of the pretrained ResNet50 model. (Zhao et al., 2017) introduced image-based CNN and data-based CNN methods for rod pump system fault diagnosis, and the results showed that CNN-based methods outperformed the traditional machine learning algorithm methods, such as the k-nearest neighbors (k-NN) and random forest (RF) methods. Besides, (Zhao et al., 2017) confirmed that image-based CNNs achieve better accuracy than data-based CNNs. Although two-dimensional signals contain more comprehensive information and can express more complex structural distributions, they also contain useless or insensitive information that can affect the diagnostic results and computational efficiency. Therefore, a 4-dimensional time-frequency signal (4D-TFS) feature extraction method that selects sensitive features from the indicator diagram is proposed to overcome the drawbacks in (**i**) by combining traditional frequency-domain and time-domain features.

The second problem is the few-shot problems. Virtual sample generation (George et al., 2017), data augmentation (Wang et al., 2018) and meta-learning (Liu et al., 2020; Munkhdalai and Yu, 2017) are commonly used solutions and have been successfully employed in target detection, image classification, and other fields. (Ren et al., 2020) developed a fault diagnosis model that uses a capsule automatic encoder to extract feature capsules, adaptively fuses them to state capsules based on a routing algorithm, and then sends them to a classifier for fault classification; this approach has fast update and few-shot learning capabilities. (Zhang and Gao, 2019) employed dictionary-based transfer learning to map data from various domains to the same subspace. The problem of incomplete data in the target domain in fault diagnosis is solved by calculating the transformation matrix of the source data of a certain well and the target data of another well and projecting the data in both domains into a subspace where each fault sample can be reconstructed by a shared dictionary. The above methods are based on few-shot samples or limited data and provide an effective solution for few-shot work condition identification. However, when facing new tasks, the network needs to be trained from scratch and cannot satisfy the real-time requirements of well identification. Model-agnostic meta-learning (MAML) (Finn et al., 2017) can learn inherent meta-knowledge among tasks during training and achieve good generalization effectiveness with a few shots of training data in new tasks (Bing, 2020; Lake et al., 2017). However, when the framework of MAML is looking for an optimal parameter that can solve multi-task optimization, it only considers the extraction of high-frequency features, but ignores the impact of low-frequency features on the performance of the model. In other words, low-frequency features are not conducive to the learning of meta-knowledge. In view of this, on the basis of the MAML framework, a ML-CSNN with a specific structure that can ablate low-frequency features is constructed in this paper for oil well workover identification of small samples to address the drawbacks in (**ii**).

In response to the above shortcomings, a working condition recognition method with few-shot samples based on 4D-TFS and ML-CSNN, which includes the two steps of low computational complexity feature extraction and few-shot working condition recognition, is proposed in this paper. The main contributions of this paper are as follows.

1) A 4D-TFS feature extraction technique is proposed for the problem of high computational complexity caused by low feature utilization of training input feature maps, and preliminary feature extraction is performed while compressing the data. The results show that the accuracy of 4D-TFS work condition recognition is better than the feature recognition accuracy of the indicator diagram, and the complexity of the algorithm is significantly reduced.
2) A convolutional shrinkage neural network (CSNN) with a specific structure that can ablate low-frequency features is established to identify well conditions. By introducing a low-frequency feature ablation mechanism, the performance of small sample condition recognition can be significantly improved.
3) A meta-learning (ML) strategy to learning meta-knowledge and fine-tune the model for new working condition types is used for the few-shot data and to address the drawback of needing to

retrain the model when new working conditions appear. The experiments demonstrate that the model has good generalization ability and can achieve accurate few-shot working condition recognition.

The remainder of this paper is organized as follows. The working condition recognition problem and few-shot learning problem are overviewed in Section 2. In Section 3, the relevant theoretical background is briefly described. The proposed working condition recognition method is elaborated in Section 4. In Section 5, the experimental comparisons are presented in detail. The conclusion and future work of this paper are summarized in Section 6.

2. Problem statement

2.1. Working condition recognition problem

The 11 most commonly known work conditions, including normal operation condition (NOC) and the following 10 fault conditions: gas interference (GIF), oil pipe leakage (OPL), continuous pumping and spraying (CPS), traveling valve leakage (TVL), insufficient liquid supply (ILS), standing valve leakage (SVL), upstroke pump bumping (UPB), sucker-rod break-off (SRB), combination of leaking standing and traveling valves (CST), and downstroke pump bumping (DPB), are investigated in this paper. As showed in Fig. 1, the horizontal axis is the displacement, and the vertical axis is the load. Each dynamometer working condition shows specific characteristics, but the shapes of some categories are also very similar, such as in Fig. 1(c) and (d), (g) and (j).

2.2. Few-shot learning problem

Compared with machine learning algorithms that usually require thousands of supervised samples to ensure their generalization ability, few-shot learning has the ability to learn and generalize from few-shot samples (Ravi and Larochelle, 2017; Santoro et al., 2016). Furthermore, given a small amount of available supervised information in dataset $\mathscr{D}_{\mathscr{T}} = \{\mathscr{D}^{tr}, \mathscr{D}^{ts}\}$ corresponding to a specific task $\mathscr{T}$, the objective of few-shot learning is to construct a function f for task $\mathscr{T}$ (Finn et al., 2019). The completion of task $\mathscr{T}$ uses little supervision information in dataset $\mathscr{D}$ to complete task $\mathscr{T}$ of mapping the input to the target. The information can be expressed as:

$$\begin{gathered}\mathscr{D}^{tr} = \{(x_i, y_i)\}_{i=1}^{N_{tr}} \\ \mathscr{D}^{ts} = \{x_j\}_{i=1}^{N_{ts}} \\ x_i, x_j \in X_\tau \subset X,\ y_i \in Y_\tau \subset Y\end{gathered} \tag{1}$$

where x represents the input data, y represents the supervision information, and X and Y represent the space of the input data and supervision information, respectively. The sample x_i, y_i used in task $\mathscr{T}$ comes from a specific domain $\mathscr{D}_{\mathscr{T}} = \{X_\tau, \mathscr{P}(X_\tau)\}$, and consists of a data space X_τ and a marginal probability distribution $\mathscr{P}(X_\tau)$.

Generally, there are N task classes in $\mathscr{D}^{tr}$, and each class has only K samples, which means the number of training data $n^{tr} = N \times K$, which is also known as an N-way K-shot. Algorithm models trained with such a small number of samples are prone to severe overfitting problems. Therefore, it is difficult to construct a high-quality model with a small amount of training data $\mathscr{D}^{tr}$.

Similarly, for the problem of identifying the working conditions of oil wells, the purpose is to generate a target prediction function $f \in F : X \to Y$ from $N \times K$ new working condition samples in training set $\mathscr{D}^{tr}$, which can be used to diagnose faults accurately and quickly from other new working condition samples in test set $\mathscr{D}^{ts}$. In addition, the problem of oil well working condition recognition is a classification problem, the loss function of which is

$$\mathscr{L}_{\mathscr{T}}(f_\theta) = \sum (\boldsymbol{x}) + (1 - \boldsymbol{y}) log(1 - f_\theta(\boldsymbol{x})) \tag{2}$$

where θ is a set of learnable parameters. The learning goal further becomes how to minimize the loss function $\mathscr{L}_{\mathscr{T}}$ using few-shot data to obtain the optimal parameters θ (Finn et al., 2019).

3. Theoretical background

3.1. CNN

A CNN is a typical feedforward neural network that has achieved outstanding results in video analysis (Wu et al., 2015), image classification (Sun et al., 2021), natural language processing (Zhao et al., 2019), target detection (Zhang et al., 2020), visual relocalization (Chen et al., 2021), and other fields. In general, the structure of a CNN is mainly composed of an input layer, an output layer and multiple hidden layers. A hidden layer is composed of a series of convolutional layers (Convs), pooling layers (Pools) and fully connected (FC) layers. By convolving the input signal, the Conv can obtain various feature maps of an activation function. For dimensionality reduction, the Pool is usually concatenated to the Conv. The category-unique local information in the Conv or Pool is consolidated into an FC layer, and the weighted sum calculation results of the one-dimensional vectors of all feature maps are provided to the FC layer. A typical CNN architecture is illustrated in Fig. 2.

3.2. Meta-learning and MAML

Meta-learning is the learning of meta-knowledge by utilizing knowledge from multiple tasks to solve the limitation of few-shot learning (Lee et al., 2019). Suppose a task is extracted from a distribution $\mathscr{T} \sim p(\tau)$, and a sequence $\mathscr{T}_i$ of I tasks is sampled from task set $\mathscr{T} = \{\mathscr{T}_1, \mathscr{T}_2, \ldots, \mathscr{T}_I\}$. In the meta-training stage, a search

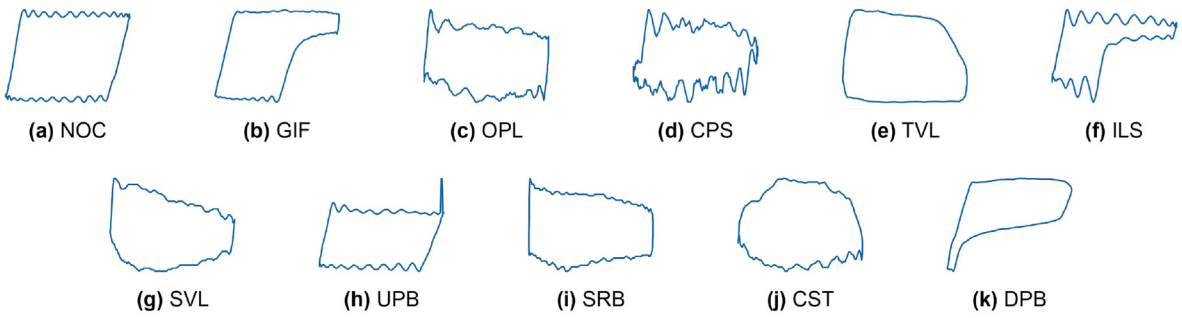

Fig. 1. Shapes of indicator diagrams under 11 different working conditions.

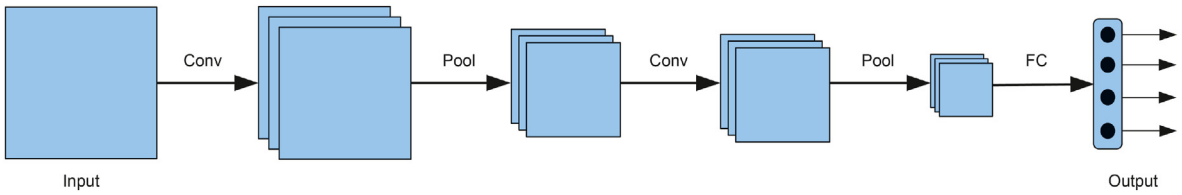

Fig. 2. Typical CNN architecture.

is performed for a meta-learner that performs well after updates to these I new tasks. In the meta-testing stage, the initialization parameters are used to fine-tune the new task $\mathscr{T}_i$ using the gradient descent method.

MAML (Finn et al., 2017) is a classic meta-learning framework that considers the meta-learner as the parameter θ. When adjusting to a new task $\mathscr{T}_i$, after one step of gradient descent, the series parameter θ of the model becomes θ_i', which takes the form of

$$\theta_i' = \theta - \alpha \nabla_\theta \mathscr{L}_{\mathscr{T}_i}(f_\theta) \tag{3}$$

where α is the inner loop learning rate. More specifically, the meta-objective is as follows:

$$\begin{aligned} \theta^* &= arg\,min_\theta \left[\sum_{\mathscr{T}_i \sim p(\tau)} \mathscr{L}_{\mathscr{T}_i}\left(f_{\theta_i'}\right) \right] \\ &= arg\,min_\theta \left[\sum_{\mathscr{T}_i \sim p(\tau)} \mathscr{L}_{\mathscr{T}_i}\left(f_{\theta - \alpha \nabla_\theta \mathscr{L}_{\mathscr{T}_i}(f_\theta)}\right) \right] \end{aligned} \tag{4}$$

where θ^* is the optimal meta-learner. In the outer loop, the stochastic gradient descent method is used to achieve meta-optimization across tasks, and the optimal model parameter θ^* is updated as follows:

$$\theta \leftarrow \theta - \beta \nabla_\theta \sum_{\mathscr{T}_i \sim p(\tau)} \mathscr{L}_{\mathscr{T}_i}\left(f_{\theta_i'}\right) \tag{5}$$

where β represents the outer loop learning rate. By continuously updating the inner and outer loop parameters, a better base model can be learned through the MAML framework.

4. Methodology

4.1. 4D-TFS feature extraction

The original working condition data of an oil well are two-dimensional closed curve charts composed of the relationship curve of the load versus displacement, as shown in Fig. 1. Normally, a two-dimensional image contains more comprehensive information than a one-dimensional signal, but the amount of calculation is too large for the parameter learning process. A traditional approach is to use the Lanczos algorithm to compress the image signal. However, considering the uniqueness of the indicator diagram data (the working condition signal is a continuous closed curve), to acquire comprehensive oil well working condition information, the working condition information should be converted and extracted preliminarily. Therefore, a 4D-TFS feature extraction method based on time-domain features and frequency-domain features is suggested in this paper. The main goal of 4D-TFS is to improve feature extraction and recognition performance by obtaining abundant information about the working conditions involved in different features extracted from various domains while reducing the computational effort in the feature extraction process. The flowchart of 4D-TFS feature extraction is shown in Fig. 3.

First, four points a, b, c and d are identified by a theoretical analysis of the indicator diagram, as shown by the red dots in Fig. 3(a); that is, the load-displacement curve is divided into four-dimensional curves (D_1, D_2, D_3, D_4). After that, according to the sampling period of a load-displacement curve, the time corresponding to each load can be obtained, and the upper stroke load $(a \rightarrow b \rightarrow c)$ and the lower stroke load $(c \rightarrow d \rightarrow a)$ are sampled by the interpolation method to obtain the load-time curve shown in Fig. 3(b). Finally, as shown in Eq. (6) and Fig. 3(c), the time-domain features TF and frequency-domain features FF of the signal are selected to form the feature set F, where F_i is the i-dimensional TF and FF, f_i^j is the j th element of the i th feature and J is the time-frequency signature length of the feature set.

$$F = [F_1 F_2 F_3 F_4]^T = \begin{bmatrix} f_1^1 & f_1^2 & \cdots & f_1^J \\ f_2^1 & f_2^2 & \cdots & f_2^J \\ f_3^1 & f_3^2 & \cdots & f_3^J \\ f_4^1 & f_4^2 & \cdots & f_4^J \end{bmatrix} \tag{6}$$

In this paper, J represents the 23 time domain and frequency domain features extracted. Specifically, 14 time-domain statistical features $TF_1 \sim TF_{14}$ and 9 frequency-domain features $FF_1 \sim FF_9$ based on the fast Fourier transform (FFT) (Cooley and Tukey, 1965) were extracted in this paper from the 4 dimensions of each signal to acquire comprehensive information about the working conditions while considering the non-negativity of the load-time curve. The basic idea of FFT algorithm uses the radix-2 butterfly block, that is, one calculates the FFT $y(k)$ of a signal $x(n)$ using Eq. (7), where W_N is the N-th twiddle factor, j is the imaginary unit, and N is the number of points of the FFT (He et al., 2021).

$$\begin{aligned} y(k) &= \sum_{n=1}^{N} x(n) \cdot W_N^{k \cdot n} \\ W_N &= e^{-j\frac{2\pi}{N}} \\ 1 \le k \le K \wedge 1 \le n \le N \end{aligned} \tag{7}$$

Statistical analysis is commonly used with extracting the characteristic information of faults and fully exploiting the state information and intrinsic properties of the original signal (Yan and Jia, 2018). For better statistical analysis in time domain, we selected all the time-domain features and the expressions are shown in Table 1. $TF_1 \sim TF_8$, TF_{15}, and TF_{16} are referred to as dimensional statistics, which are mean value, root-mean-square value, square root amplitude, variance, maximum value, minimum value, peak-to-peak value, standard deviation, absolute mean value, and peak value, respectively, and $TF_9 \sim TF_{14}$ are called dimensionless statistics, which are peak factor, mean waveform factor, margin factor, pulse factor, skewness factor, and kurtosis factor, respectively (Decker, 2002; Liu et al., 2013, 2019; Pvc et al., 2005; Yan and Jia,

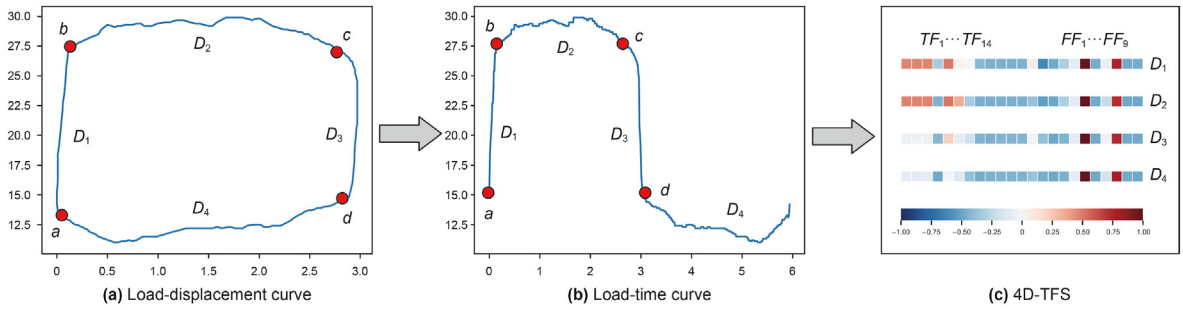

Fig. 3. Flowchart of 4D-TFS feature extraction.

Table 1
Time-domain feature expressions.

Feature expression	Feature expression	Feature expression	Feature expression
$TF_1 = \frac{1}{N}\sum_{n=1}^{N} x(n)$	$TF_5 = \max(x(n))$	$TF_9 = \frac{TF_{16}}{TF_2}$	$TF_{13} = \frac{\frac{1}{N}\sum_{n=1}^{N}(x(n)-TF_1)^3}{(TF_8)^3}$
$TF_2 = \sqrt{\frac{1}{N}\sum_{n=1}^{N}(x(n))^2}$	$TF_6 = \min(x(n))$	$TF_{10} = \frac{TF_2}{TF_{15}}$	$TF_{14} = \frac{\frac{1}{N}\sum_{n-1}^{N}(x(n)-TF_1)^4}{(TF_4)^2}$
$TF_3 = \left(\frac{1}{N}\sum_{n=1}^{N}\sqrt{\lvert x(n)\rvert}\right)^2$	$TF_7 = TF_5 - TF_6$	$TF_{11} = \frac{TF_{16}}{TF_3}$	$TF_{15} = \frac{1}{N}\sum_{n=1}^{N}\lvert x(n)\rvert$
$TF_4 = \frac{1}{N}\sum_{n=1}^{N}(x(n)-TF_1)^2$	$TF_8 = \sqrt{TF_4}$	$TF_{12} = \frac{TF_{16}}{TF_{15}}$	$TF_{16} = \max\lvert x(n)\rvert$

2018). $x(n), n = 1, 2, 3, \ldots, N$ is the time series, where N is the length of signal u (Yu et al., 2021). In this paper, the first 14 time-domain feature expressions are selected in view of the non-negativity of the load-time curve in Fig. 3(b), i.e., $x(n) > 0$.

The calculation of statistical features is an effective tool for feature extraction. To achieve greater statistical analysis in the frequency domain, the expressions of all frequency domain statistical features are shown in Table 2. The feature FF_1 denotes the magnitude of the vibration energy in the frequency domain, the features $FF_2 \sim FF_5$, FF_9, $FF_{11} \sim FF_{13}$ represent the dispersion of the spectrum, and the features $FF_6 \sim FF_8$, FF_{10} indicate the main frequency band position change (Decker, 2002; Liu et al., 2013, 2019; Pvc et al., 2005; Yan and Jia, 2018). $y(k), k = 1, 2, \cdots, K$ is the FFT spectrum of the given signal $x(n)$, K is the number of spectrum lines and f_k is the frequency value of the k th spectrum line (Yu et al., 2021). Due to some frequency domain features $FF \rightarrow 0$ or ∞, only the first 9 frequency domain features are selected to construct the TFS in this paper.

Interestingly, we can also divide the load-displacement curve in Fig. 3 into 1, 2 or 8 parts to form 1D-TFS, 2D-TFS, and 8D-TFS respectively. The relevant experimental results are described in Appendix accordingly.

4.2. CSNN

Different from traditional CNNs, convolutional shrinkage neural networks (CSNNs) add specific shrinkage modules to ablate low-frequency features. The noise is suppressed by the introduction of a low-frequency feature ablation mechanism, and the correlation between high- and low-frequency features is enhanced. The shrinkage refers to soft thresholding.

Soft thresholding (Isogawa et al., 2018; Zhao et al., 2020) is a central step in many signal noise reduction methods. Features with absolute values less than a certain threshold τ are set to zero, and features larger than that threshold τ are reduced to zero. The soft threshold function can be formulated as:

Table 2
Frequency-domain feature expressions.

Feature expression	Feature expression	Feature expression	Feature expression
$FF_1 = \frac{\sum_{k=1}^{K} y(k)}{K}$	$FF_5 = \sqrt{\frac{\sum_{k=1}^{K}[(f_k - FF_{10})^2 y(k)]}{K}}$	$FF_9 = \frac{\sum_{k=1}^{K}[\sqrt{\lvert f_k - FF_{10}\rvert}y(k)]}{K\sqrt{FF_5}}$	$FF_{13} = \frac{\sum_{k=1}^{K}[(f_k - FF_{10})^4 y(k)]}{K(FF_5)^4}$
$FF_2 = \frac{\sum_{k=1}^{K}[y(k) - FF_1]^2}{K-1}$	$FF_6 = \sqrt{\frac{\sum_{k=1}^{K}(f_k^2 y(k))}{\sum_{k=1}^{K} y(k)}}$	$FF_{10} = \frac{\sum_{k=1}^{K}(f_k y(k))}{\sum_{k=1}^{K} y(k)}$	–
$FF_3 = \frac{\sum_{k=1}^{K}[y(k) - FF_1]^3}{K(\sqrt{FF_2})^3}$	$FF_7 = \sqrt{\frac{\sum_{k=1}^{K}(f_k^4 y(k))}{\sum_{k=1}^{K}(f_k^2 y(k))}}$	$FF_{11} = \frac{FF_5}{FF_{10}}$	–
$FF_4 = \frac{\sum_{k=1}^{K}[y(k) - FF_1]^4}{K(FF_2)^2}$	$FF_8 = FF_6\sqrt{\frac{\sum_{k=1}^{K}(f_k^2 y(k))}{\sum_{k=1}^{K}(f_k^4 y(k))}}$	$FF_{12} = \frac{\sum_{k=1}^{K}[(f_k - FF_{10})^3 y(k)]}{K(FF_5)^3}$	–

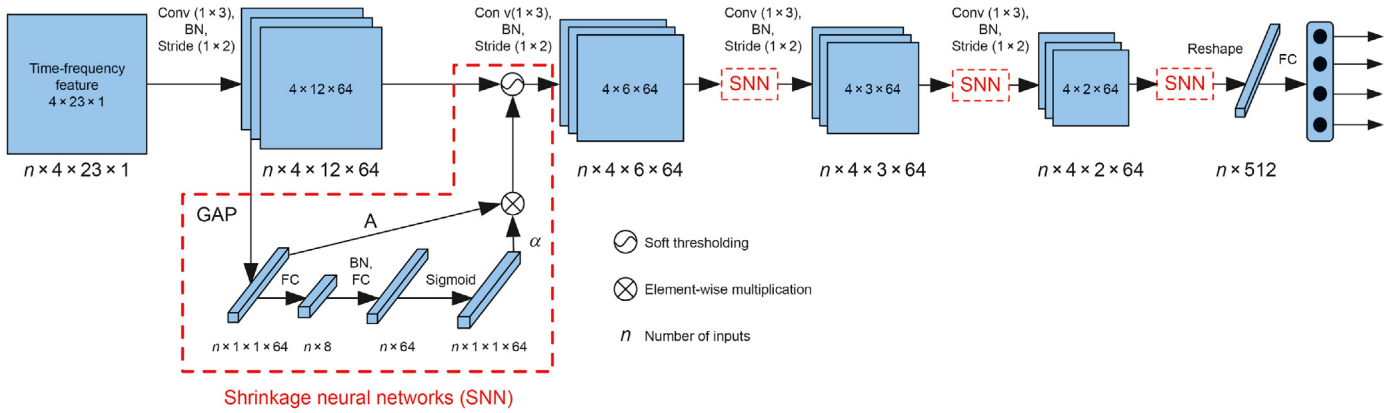

Fig. 4. A specific architecture of a CSNN.

$$y = \begin{cases} x - \tau, & x > \tau \\ 0, & 0 \le x \le \tau \end{cases} \tag{8}$$

where $\boldsymbol{x}$ and $\boldsymbol{y}$ are the input feature and the output feature, respectively, and $\boldsymbol{\tau}$ is the threshold value. From Eq. (8), it can be seen that soft thresholding can set the features of any interval to zero, and it is a more flexible method to eliminate features in a certain value range.

The network structure of the complete CSNN is shown in Fig. 4. In the shrinkage neural network (SNN), the absolute values of all the features in the input feature map are first found. After global average pooling (GAP), a feature is obtained and represented as A. Moreover, the feature map after GAP is fed into a small FC network. The FC network takes the sigmoid function as the last layer and obtains a coefficient α normalized to 0 and 1. The final threshold can be denoted as $\alpha \times A$. In this way, it is ensured that the obtained noise threshold is not only positive but also not too large. Therefore, the SNN can be understood to some extent as a special attention mechanism: when it notices noisy features that are not related to the current task, it sets them to zero by soft thresholding, and they are retained when recording features that are associated with the current task.

With the sigmoid function, the output of the FC network can be scaled to the range of 0–1 and can be represented as:

$$\alpha_i = \frac{1}{1 + e^{-z_i}} \tag{9}$$

where α_i is the i th scaling parameter and z_i is the FC network output feature of the i th neuron. The threshold values used in the SNN are denoted as follows:

$$\tau_i = \alpha_i \bullet Average\left|x_{w,h,i}\right| \tag{10}$$

where w and h are the width and height, respectively, i is the channel of the feature map x, and τ_i is the threshold value of the i th channel of the feature map.

4.3. ML-CSNN for working condition recognition

With the extraction of 4D-TFS features and the construction of the CSNN, the ML-CSNN can be trained for well working condition recognition. Fig. 4 specifies the architecture of the proposed ML-CSNN. The feature size of the input layer is $4 \times 23 \times 1$. The network consists of 4 successive convolutional layers, 4 SNNs and 1 FC layer with 1×3 and 1×2 filters that use 64 channels. The number of FC layer neurons is 4.

Based on the meta-learning research results, the ML-CSNN, which is a few-shot working condition recognition model, is proposed in this paper. In the ML-CSNN, the meta-learning strategy of MAML is presented. The main idea is to let the designed CSNN learn to learn; i.e., the model only needs a small number of training iterations and a small amount of sample ($N \times K$ sample) data to quickly adapt to a new working condition recognition task.

It is assumed that f_θ is the ML-CSNN model, θ is the initial model parameter, and θ^* is the optimal model parameter. The algorithm scheme of the proposed ML-CSNN is illustrated in Algorithm 1.

Algorithm 1. ML-CSNN for Few-shot Working Condition Recognition

Require: $p(\tau)$: distribution over tasks
Require: α, β: step size hyperparameters
1: Randomly initialize θ of the ML-CSNN
2: **while** not done **do**
3: Sample batch of tasks $\mathcal{T}_i \sim p(\tau)$
4: **for all** $\mathcal{T}_i$ **do**
5: Sample $N \times K$ datapoints $\mathcal{D} = \{x, y\}$ from $\mathcal{T}_i$
6: Evaluate $\nabla_\theta \mathcal{L}_{\mathcal{T}_i}(f_\theta)$ using $\mathcal{D}$ and $\mathcal{L}_{\mathcal{T}_i}$ through Eq. (2)
7: Compute the adapted parameters with gradient descent through Eq. (3)
8: Sample $N \times K$ datapoints $\mathcal{D}_i' = \{x, y\}$ from $\mathcal{T}_i$ for the meta-update
9: **end for**
10: Update θ^* using $\mathcal{D}_i'$ and $\mathcal{L}_{\mathcal{T}_i}$ through Eq. (2) and Eq. (5)
11: **end while**

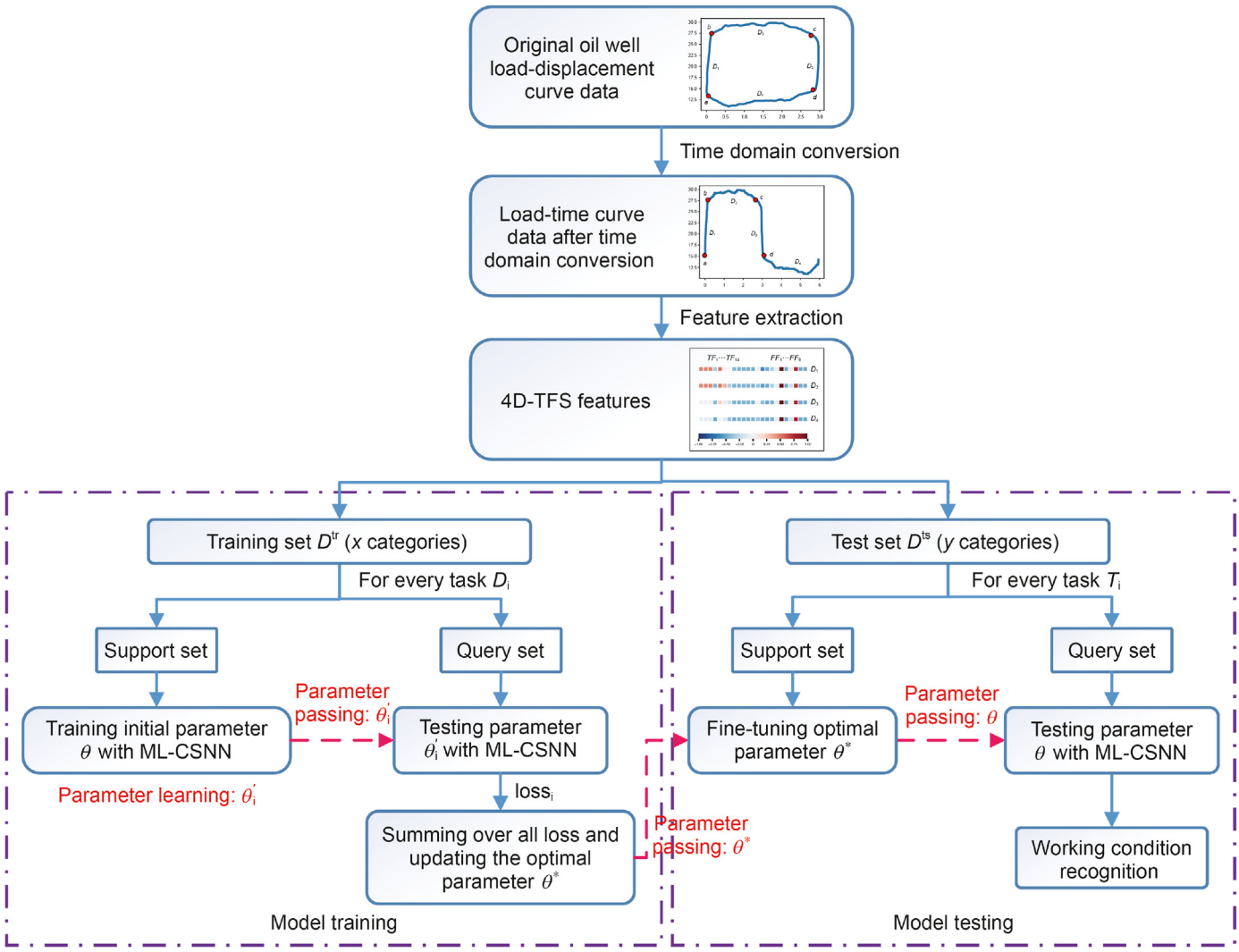

Fig. 5. Flowchart of few-shot working condition recognition based on 4D-TFS and the ML-CSNN.

With the 4D-TFS features and ML-CSNN as the premise, the flowchart of the proposed oil well few-shot working condition identification method in this paper is illustrated in Fig. 5. The general steps of the proposed method are summarized as follows.

1) The indicator diagram data (load-displacement curve data) of the oil well are obtained, the load-time curve data are further obtained by a time-domain conversion, and then the 4D-TFS features of the load-time curve are extracted. Subsequently, the dataset is divided into training and test sets without category repetition.
2) The training task set $\mathscr{T}_i$ and the test task set $\mathscr{T}_j$ are generated using the training set $\mathscr{D}^{tr}$ and the test set $\mathscr{D}^{ts}$, respectively. Each subtask contains support sets and query sets.
3) The ML-CSNN is trained by using a training subtask set to acquire optimal parameters θ^* that are sensitive to task changes, which are passed to the test subtask set.
4) The network parameter θ^* is fine-tuned with the support set in the test subtask set $\mathscr{T}_j$, and the corresponding query set is utilized to perform few-shot working condition recognition.

5. Experimental evaluation

5.1. Experimental platform and data collection

The developed 4D-TFS ML-CSNN is implemented using TensorFlow 1.14.0, which is a machine learning toolkit released by Google. All the experimental results are obtained by a computer with an i7–10700k CPU and 32 GB RAM.

The oil well data used in this experiment are sourced from an existing oil field in northern China. The data are collected periodically by sensors mounted on the pumping rods. We use only the displacement and load data to generate indicator diagrams for analyzing the pumping conditions. In addition, for the electrical parameter data, the data vacancy values are filled by finding the average value under the attribute to which it belongs, the data used are constrained in the form of data constraints, and the data noise is suppressed using the split-box method most typical of data discretization.

Generally, the wells are mostly in normal operating conditions and it is difficult to get multiple fault operating conditions on a

single well, so we collected data from nearly 1300 wells for more than 90 days. This data contains multiple failure types, and we selected 11 typical working conditions (as shown in Fig. 1) with high sample size for the experiment. As the working condition data are collected from different wells in the field, we used the Min-Max normalization method to normalize the collected displacement and load data in order to eliminate the differences between different wells.

$$L_i^* = \frac{L_i - min(L)}{max(L) - min(L)} \tag{11}$$

$$D_i^* = \frac{D_i - min(D)}{max(D) - min(D)} \tag{12}$$

where L_i^* and D_i^* are the normalized load and displacement data, for $i = 1, 2, \ldots, 200$, and $min(L), max(L), min(D)$ and $max(D)$ are the minimum load, maximum load, minimum displacement and maximum displacement, respectively (Cheng et al., 2020).

It is important to reiterate that the working condition categories for the training and test sets are completely different. For each working condition category, 5000 samples are screened. To follow the typical experimental N-way K-shot scheme (Vinyals et al., 2016) and considering the small number of working condition types, 4-way 1-shot and 4-shot experiments are conducted in this paper, which means that $4 \times K$ labeled samples are used for training and new samples of the same working conditions are used for testing while obtaining good classification ability. More specifically, 5000 labeled samples for each work condition category are used to train the model during the model training phase. And in the model testing phase, only K (1 or 4) samples of the new working conditions used to fine-tune the model have known labels, and the remaining $5000 - K$ samples are used to test the recognition accuracy of "few-shot" model.

5.2. 4D-TFS feature extraction of a sucker-rod pumping system

In the 4D-TFS feature extraction stage, each complete load-time curve is divided into 4 segments with no overlap points between segments. In the time-domain conversion stage of the indicator diagram, the sampling period is set to 0.01 s. The length of each time-domain signal segment is also the input length when extracting the frequency- and time-domain features. To ensure the reliability of the outcome, normalization is applied in the 4D-TFS feature extraction process.

The indicator diagram method has been successfully applied to the identification of sucker-rod pumping system conditions. Inspired by this, a comparison of the indicator diagram method and the proposed method is studied. The size of the original indicator diagram in this paper is 640×480, and the image signal is compressed to 32×24 using the Lanczos algorithm. Based on the 4-way 4-shot task, 4 fault categories are randomly selected from the dataset containing 11 working condition types for 4D-TFS and indicator diagram feature extraction.

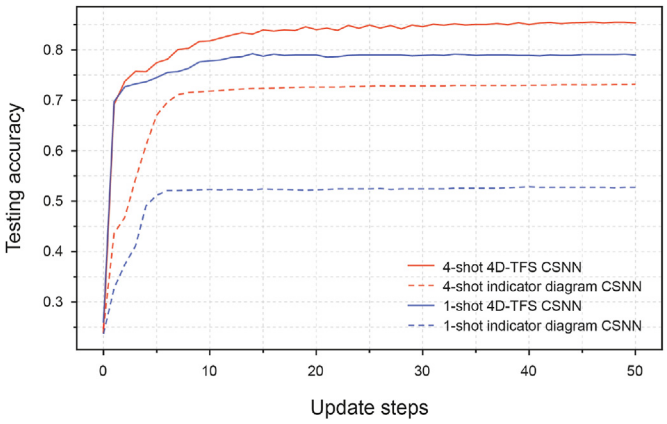

Fig. 6. Accuracy of 2 feature extraction methods with different numbers of update steps.

Table 4
CSNN algorithm indicators.

Feature extraction method	indicator diagram	4D-TFS
Feature map size	32×24	4×23
Param, MB	46.08	44.40
FLOPs, GB	7.07	4.68

The accuracy of these features in identifying the few-shot working conditions was assessed using the CSNN, as shown in Fig. 4. Different from 4D-TFS, for the indicator diagram, the input size is 32×24, and the convolution kernel and step size are 3×3 and 2×2, respectively. K-shot samples of each condition category are trained and tested with the CSNN during the work condition recognition process. To prevent results that occur due to chance and specificity, the experiment was replicated 300 times, and the average results are shown in Table 3.

As seen from Table 3 and Fig. 6, the 4D-TFS method proposed in this paper has good results compared with the indicator diagram method, and the accuracy of 4D-TFS can reach 85.35% for the same number of update steps. That is, with the same classifier, 4D-TFS can achieve more discriminative features that are critical for working condition recognition compared with the indicator diagram method, thus obtaining higher recognition accuracy, which also demonstrates the high sensitivity of 4D-TFS for few-shot work condition recognition. In addition, Fig. 6 shows that the accuracy of

Table 5
Details of the dataset partition.

Dataset	Number of training categories	Number of test categories
Dataset A	4	7
Dataset B	5	6
Dataset C	6	5
Dataset D	7	4

Table 3
Working condition recognition accuracies based on different feature extraction methods using the CSNN.

Feature extraction method		indicator diagram	4D-TFS
Accuracy (step = 10)	1-shot	52.33 ± 2.73%	77.83 ± 2.19%
	4-shot	71.81 ± 1.61%	81.77 ± 1.66%
Accuracy (step = 20)	1-shot	52.25 ± 2.78%	79.00 ± 2.25%
	4-shot	72.60 ± 1.60%	84.02 ± 1.54%
Accuracy (step = 50)	1-shot	52.75 ± 2.79%	79.00 ± 2.29%
	4-shot	73.17 ± 1.56%	85.35 ± 1.44%

the model has basically reached a stable value after 20 update steps for both the indicator diagram and the 4D-TFS feature extraction methods. Therefore, the number of iterations for the following experiments is uniformly set to 20 in this paper.

Additionally, Table 4 shows the impact of two different feature extraction methods on the CSNN performance. It is obvious that 4D-TFS has a significant improvement in both time complexity and algorithm complexity, especially in algorithm complexity; the complexity of 4D-TFS is only 66.20% of that of the indicator diagram method. Through the analysis of Table 3, Table 4, and Fig. 6, the rationality of the solution proposed to solve the first problem is preliminarily verified.

5.3. Few-shot working condition recognition based on meta-learning

This section validates the performance of the ML-CSNN in few-shot working condition recognition. As shown in Table 5, the datasets were divided into training and test sets at different scales.

In the model training phase, the training step number is set to 10000, and the number of subtasks in the meta-learning task is 4. To reduce the computational effort, the update step of the subtask is set to 10. The meta-task learning rate is 0.001, and the subtask learning rates of 4D-TFS and the indicator diagram method are 0.01 and 0.2, respectively. Furthermore, 200000 training subtasks are generated using the training set. In the training process of each subtask, 4 classes are randomly extracted from the training set, K samples from each class are taken to form the subtask support set, and another K new samples are taken to form the query set. In the model testing phase, 600 test subtasks are generated from the test set with the same parameter settings as those in the training subtasks. The network is fine-tuned using the support set in each subtask, and the optimal parameters $\theta^{*\prime}$ of the fine-tuned network are acquired. The query set samples are then input to the neural network to realize few-shot working condition recognition. Different from the model training phase, the update step of the subtask is set to 20 at this time. Finally, the accuracy of all test subtasks is averaged to obtain the test accuracy of the final experiment.

5.3.1. Few-shot working condition recognition based on 4D-TFS and ML-CSNN

Few-shot working condition recognition of pumping wells under the two scenarios of 4-way 1-shot and 4-way 4-shot using datasets A, B, C and D is performed. The test results for the two scenarios under the four datasets are shown in Fig. 7, and the final accuracy after 10000 training and 20 update steps are displayed in Table 6.

Table 6
Working condition recognition accuracies based on 4D-TFS and the ML-CSNN.

Dataset	4-way 1-shot	4-way 4-shot
Dataset A	83.83 ± 2.74%	89.31 ± 1.35%
Dataset B	87.00 ± 2.34%	92.83 ± 1.01%
Dataset C	87.08 ± 2.33%	92.10 ± 0.96%
Dataset D	88.92 ± 2.20%	94.08 ± 0.87%

As shown in Fig. 7 and Table 6, it is obvious that with the same dataset, when the number of training samples is increased from 1-shot to 4-shot, the model's working condition recognition accuracy is greatly improved. In the case where the support set is a 4-way 1-shot, as the types of sampling working conditions decrease during training, the accuracy of working condition recognition decreases to varying degrees. Interestingly, under the 4-way 4-shot task, the accuracy on dataset B is higher than that on dataset C. This may be caused by the fact that the characteristics of the samples in each category are different. The above analysis is identical to the fact that reducing the number of training samples or working condition categories increases the difficulty of working condition identification.

In addition, on dataset D, the recognition accuracies of the ML-CSNN for the 1-shot and 4-shot tasks are 88.92% and 94.08%, respectively, which are much higher than the 79.00% and 85.35% accuracies of the CSNN, as illustrated in Table 3. The results demonstrate that the trained model has higher recognition accuracies for different few-shot tasks. Even if the types of working conditions for training (dataset D → dataset A) are reduced and the difficulty of working condition recognition is increased, the accuracy of the ML-CSNN model is still higher than that of the CSNN, demonstrating that the proposed ML-CSNN model has strong fast learning and generalization capabilities. The above analysis also verifies the effectiveness of the MAML framework used in this paper for few-shot learning and provides a solution to the second problem.

5.3.2. Few-shot working condition recognition based on an indicator diagram and the ML-CSNN

To further validate the effectiveness of the proposed 4D-TFS feature extraction method under the meta-learning strategy, an

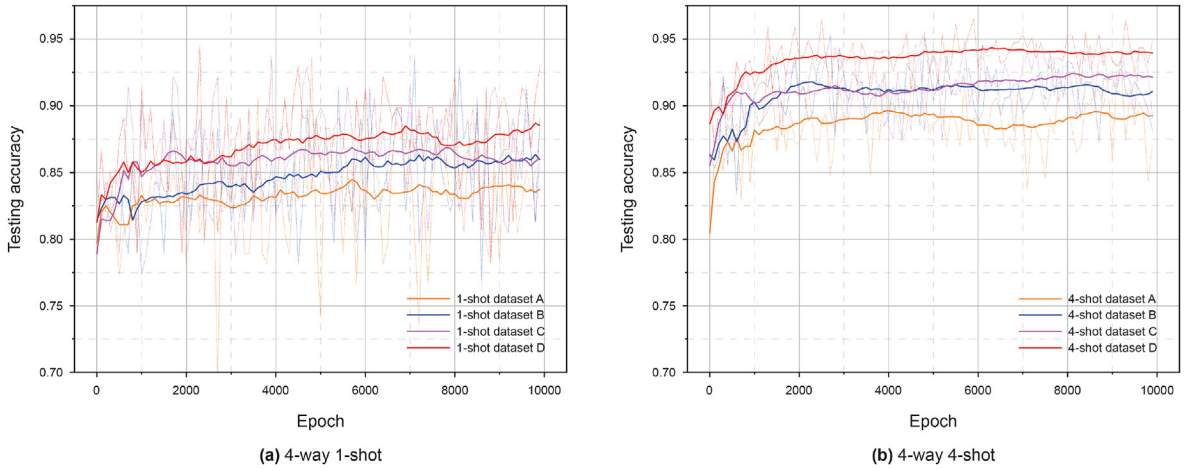

(a) 4-way 1-shot **(b)** 4-way 4-shot

Fig. 7. Working condition recognition accuracies for the 4-way 1-shot and 4-shot tasks.

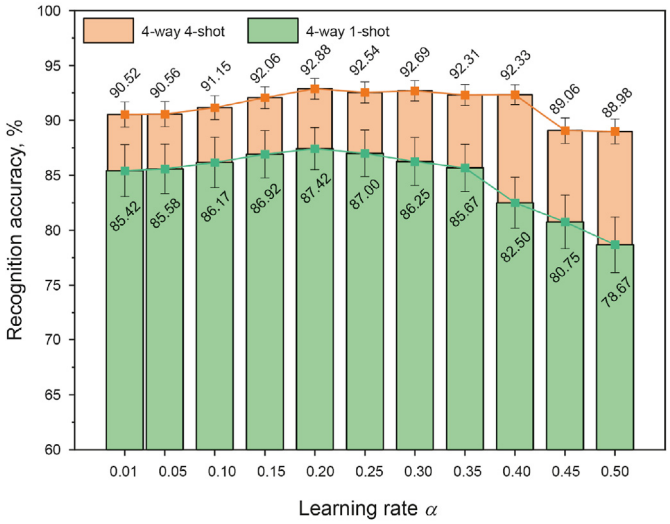

Fig. 8. The 4-way 1-shot and 4-shot recognition accuracies with different learning rates α when using dataset D.

Table 7
Working condition recognition accuracies based on the indicator diagram method and the ML-CSNN.

Dataset	4-way 1-shot	4-way 4-shot
Dataset A	81.42 ± 2.41%	84.92 ± 1.51%
Dataset B	88.09 ± 1.94%	90.83 ± 1.06%
Dataset C	87.00 ± 2.06%	91.13 ± 1.02%
Dataset D	87.42 ± 1.91%	92.88 ± 0.95%

indicator diagram is used as input for comparison. Unlike in Section 5.2, the ML-CSNN strategy is used instead of the CSNN framework alone.

It is well known that the learning rate is the most important hyperparameter. When the learning rate is too large, gradient descent may inadvertently increase the training error. When the learning rate is too small, training is not only slow, but may also be permanently stuck at a local minimum (Goodfellow et al., 2016). Unfortunately, we cannot analytically compute the optimal learning rate for a given model on a given dataset. Instead, a good learning rate must be discovered through iterative trials. According to the empirical value setting, the 4-way 1-shot and 4-way 4-shot

Table 8
Working condition recognition accuracies based on 4D-TFS and the MAML.

Dataset	4-way 1-shot	4-way 4-shot
Dataset A	84.42 ± 2.46%	88.56 ± 1.27%
Dataset B	86.75 ± 2.23%	92.00 ± 1.04%
Dataset C	85.17 ± 2.52%	90.44 ± 1.09%
Dataset D	88.83 ± 2.05%	93.77 ± 0.90%

recognition accuracies with different learning rates α when using dataset D are shown in Fig. 8. Obviously, the best classification accuracy of 87.58% and 92.88% is obtained for 1-shot and 4-shot, respectively, when the learning rate is 0.2, and the classification stability is also the best.

The work condition recognition accuracies for the different datasets of the two tasks are presented in Table 7. Fig. 9 exhibits the work condition recognition accuracies of the 2 feature extraction methods with different training steps. From the comparisons in Fig. 9 and Tables 6 and 7, it is obvious that the 4D-TFS feature extraction approach outperforms the indicator diagram approach in terms of work condition recognition accuracy with the ML-CSNN strategy both in the 4-way 1-shot and 4-shot tasks, which also illustrates that 4D-TFS has better model recognition under few-shot conditions. In addition, Table 3 also verifies the reasonableness of the proposed solution for the first problem.

5.3.3. *Few-shot working condition recognition based on 4D-TFS and MAML*

For the second question, this section uses 4D-TFS as input, and the MAML strategy is used for comparison. Unlike the ML-CSNN strategy, the MAML does not insert the SNN module; i.e., the MAML directly uses a normal CNN network architecture without introducing a soft thresholding mechanism to ablate the low-frequency features. Table 8 depicts the work condition recognition accuracies for the different datasets under the two tasks. Fig. 10 displays the comparison of the working condition recognition accuracies of the ML-CSNN and MAM strategies with different training steps.

The accuracy comparisons of working condition recognition in Fig. 10 and Tables 6 and 8 demonstrate that the working condition recognition performance of the ML-CSNN strategy is better than that of the MAML strategy on the same dataset and few-shot task, especially the 4-shot task. This indicates that the performance of well condition recognition under small sample conditions can also

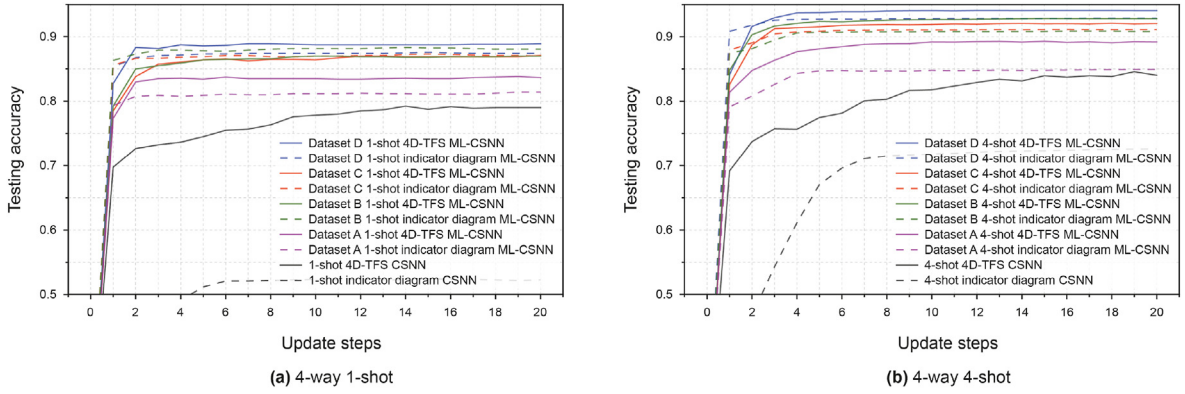

(a) 4-way 1-shot **(b)** 4-way 4-shot

Fig. 9. Working condition recognition accuracies of different feature extraction methods for the 4-way 1-shot and 4-shot tasks.

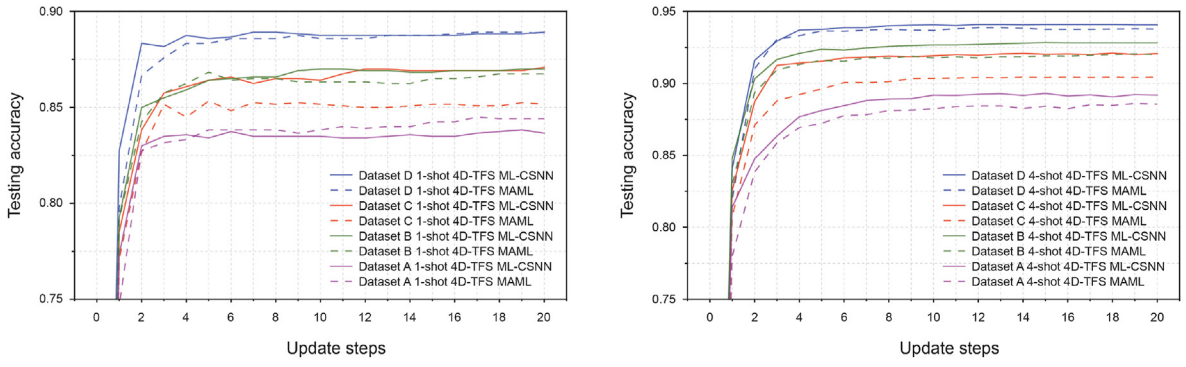

(a) 4-way 1-shot **(b)** 4-way 4-shot

Fig. 10. Working condition recognition accuracies of the different strategies for the 4-way 1-shot and 4-shot tasks.

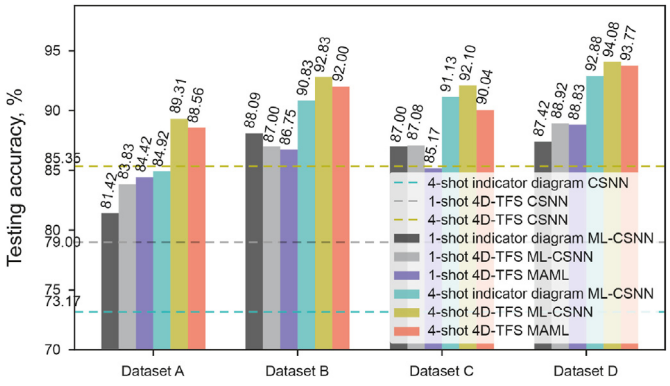

Fig. 11. Working condition recognition accuracies of various proposed strategies.

be improved by introducing a low-frequency feature ablation mechanism to ablate low-frequency features, thus verifying the effectiveness of the solution for the second problem proposed in this paper.

5.4. Discussion

To evaluate the performance of the various solutions presented in this paper as a whole and to facilitate the comparison of the working condition identification results of the various solutions, Fig. 11 exhibits the well working condition recognition accuracies of the various strategies on different datasets and different small sample tasks.

The results in Fig. 11 show that the accuracy of the 4D-TFS feature extraction method is better than that of the indicator diagram method with the same ML-CSNN or CSNN strategy, except for the recognition accuracy of the 1-shot task when using dataset B. For example, using dataset D and ML-CSNN strategies, under the conditions of 4-way 4-shot, the accuracy of the indicator diagram as input is 91.96%, while the accuracy of 4D-TFS is 94.08%, which is 2.12% higher than the accuracy of the indicator diagram. This confirms the high sensitivity of 4D-TFS features for the recognition of the few-shot working state. Moreover, it can be concluded from Table 4 that 4D-TFS can compress the data, which reduces the computational complexity to 66.20% compared with the indicator diagram. Hence, the first problem is solved successfully.

Second, the fine-tuning strategy using meta-learning, i.e., the ML-CSNN architecture, achieves higher work condition recognition accuracy than the CSNN architecture without meta-learning with the same feature extraction method and *K*-shot task. For example, using 4D-TFS as input, under the few-shot sample condition of 4-way 4-shot, the accuracy of CSNN is 85.35%, and the accuracy of ML-CSNN architecture under dataset D is 94.08%, which is 8.73% higher than the accuracy of CSNN without the meta-learning strategy. This verifies that the trained model can achieve highly accurate few-shot work condition recognition with fewer samples and iterations. Finally, the overall accuracy of the ML-CSNN architecture is better than that of the MAML architecture using 4D-TFS features as input. For example, using dataset B and 4D-TFS as input, under 4-way 4-shot conditions, the accuracy of the MAML architecture is 92.00%, while the accuracy of the ML-CSNN architecture is 92.83%, which is 0.83% higher than the accuracy of MAML. This indicates that the soft thresholding mechanism can effectively improve the accuracy of working condition recognition for few-shot tasks by ablating low-frequency features, which also verifies the effectiveness of the proposed improvement scheme to solve the second problem. Hence, the second problem proposed in the paper is successfully solved.

6. Conclusions and future work

In this paper, a few-shot working condition recognition method for a sucker-rod pumping system based on 4D-TFS and the ML-CSNN is proposed and realizes few-shot working condition recognition with the ML-CSNN after the load-displacement curve is converted to the time-domain and the 4D-TFS features of the load-time curve are extracted. The results of the experiments show that the method can realize few-shot new working condition identification of oil wells with great recognition accuracy and good generalization ability, and therefore, it is of great significance for the rapid diagnosis of new working conditions with few samples in the late stage of oilfield exploitation and the rapid identification of operating conditions for new oil wells.

The 4D-TFS with integrated working condition information is more sensitive to few-shot working condition recognition than the traditional two-dimensional indicator diagram, and there is a significant reduction in computational effort. In addition, compared with the classic MAML framework, the ML-CSNN introduces a low-frequency feature ablation mechanism SNN, which can achieve more accurate few-shot samples work condition recognition results. Finally, the ML-CSNN has a strong fast learning capability, which means that only few-shot samples and updates are needed to fine-tune the network to quickly adapt to new work conditions. The experiments indicate that the proposed method is useful for the rapid

identification of new working conditions of actual sucker-rod pumping systems.

However, due to condition limitations, only 11 common working conditions are collected in this paper, while the number of actual well working conditions can be more than 20. The generalization performance will be stronger if more categories of working condition data are collected to train the model, which means that the few-shot sample fault diagnosis performance higher than 94.08% under new working conditions can be obtained in practical applications. In addition, 4D-TFS, as a novel feature extraction method for indicator diagrams, 23 time domain and frequency domain features are selected in this paper for feature extraction, and each feature has a different impact on the performance of small sample working condition recognition. Therefore, selecting and optimizing the 23 fusion time-frequency features is also the next research content.

Declaration of competing interest

The authors declare that they have no known competing financial interests or personal relationships that could have appeared to influence the work reported in this paper.

Acknowledgements

We would like to thank the associate editor and the reviewers for their constructive comments. This work was supported in part by the National Natural Science Foundation of China under Grant U1908212, 62203432 and 92067205, in part by the State Key Laboratory of Robotics of China under Grant 2023-Z03 and 2023-Z15, also in part by the Natural Science Foundation of Liaoning Province under Grant 2020-KF-11-02.

A. Appendix

Table 9 shows the accuracy of working condition recognition based on ML-CSNN under different time-frequency signals (TFS). Obviously, dividing the load-displacement curve into 1 part, and 2 parts respectively forming 1D-TFS and 2D-TFS can not extract enough characteristic information for working condition recognition, which reduces the accuracy of small sample working condition recognition. However, splitting the load-displacement curve too much is also not conducive to improving the recognition accuracy. This is because the load-displacement curve data is only composed of 200 points, and too few sample points will cause the time-frequency feature extraction effect to be poor, which reduces the 8D-TFS recognition accuracy.

References

Bing, X., 2020. Critical infrastructure protection based on memory-augmented meta-learning framework. Neural Comput. Appl. 32 (23), 17197–17208. https://doi.org/10.1007/s00521-020-04760-7.

Chen, Z., Pei, H., Wang, J., Dai, D., 2021. Survey of monocular camera-based visual relocalization. Robot 43 (3), 373–384. https://doi.org/10.13973/j.cnki.robot.200350.

Cheng, H., et al., 2020. Automatic recognition of sucker-rod pumping system working conditions using dynamometer cards with transfer learning and svm. Sensors-Basel 20 (19), 1–15. https://doi.org/10.3390/s20195659.

Cooley, J.W., Tukey, J.W., 1965. An algorithm for the machine calculation of complex fourier series. Math. Comput. 19 (90), 249–259. https://doi.org/10.1090/S0025-5718-1965-0178586-1.

Decker, H.J., 2002. Crack Detection for Aerospace Quality Spur Gears. Crack Detection for Aerospace Quality Spur Gears. https://ntrs.nasa.gov/citations/20020061785.

Finn, C., Abbeel, P., Levine, S., 2017. Model-agnostic meta-learning for fast adaptation of deep networks. In: 34th International Conference on Machine Learning. ICML, pp. 1856–1868. https://doi.org/10.48550/arXiv.1703.03400, 2017.

Finn, C., Rajeswaran, A., Kakade, S., Levine, S., 2019. Online meta-learning. In: 36th International Conference on Machine Learning. ICML, pp. 3398–3410. https://doi.org/10.48550/arXiv.1902.08438, 2019.

George, D., et al., 2017. A generative vision model that trains with high data efficiency and breaks text-based CAPTCHAs. Science 358 (6368). https://doi.org/10.1126/science.aag2612.

Goodfellow, I., Bengio, Y., Courville, A., 2016. Deep Learning. MIT Press, p. 424, 424. https://www.deeplearningbook.org.

Han, Y., Li, K., Ge, F., Wang, Y., Xu, W., 2021. Online Fault Diagnosis for Sucker Rod Pumping Well by Optimized Density Peak Clustering. ISA T. https://doi.org/10.1016/j.isatra.2021.03.022.

He, Y., et al., 2021. Rolling bearing fault diagnosis based on meta-learning with few-shot samples. In: 2021 3rd International Conference on Industrial Artificial Intelligence (IAI), pp. 1–6. https://doi.org/10.1109/IAI53119.2021.9619308.

Isogawa, K., Ida, T., Shiodera, T., Takeguchi, T., 2018. Deep shrinkage convolutional neural network for adaptive noise reduction. IEEE Signal Process. Lett. 25 (2), 224–228. https://doi.org/10.1109/LSP.2017.2782270.

Lake, B.M., Ullman, T.D., Tenenbaum, J.B., Gershman, S.J., 2017. Building machines that learn and think like people. Behav. Brain Sci. 40, 25. https://doi.org/10.1017/s0140525x16001837.

Lee, K., Maji, S., Ravichandran, A., Soatto, S., 2019. Meta-learning with differentiable convex optimization. In: 32nd IEEE/CVF Conference on Computer Vision and Pattern Recognition. https://doi.org/10.1109/CVPR.2019.01091. CVPR 2019.

Li, K., Gao, X.-w., Yang, W.-b., Dai, Y.-l., Tian, Z.-d., 2013a. Multiple fault diagnosis of down-hole conditions of sucker-rod pumping wells based on Freeman chain code and DCA. Petrol. Sci. 10 (3), 347–360. https://doi.org/10.1007/s12182-013-0283-4.

Li, K., Gao, X., Tian, Z., Qiu, Z., 2013b. Using the curve moment and the PSO-SVM method to diagnose downhole conditions of a sucker rod pumping unit. Petrol. Sci. 10 (1), 73–80. https://doi.org/10.1007/s12182-013-0252-y.

Li, K., Gao, X.W., Zhou, H.B., Han, Y., 2015. Fault diagnosis for down-hole conditions of sucker rod pumping systems based on the FBH–SC method. Petrol. Sci. 12 (1), 135–147. https://doi.org/10.1007/s12182-014-0006-5.

Li, K., Han, Y., Wang, T., 2018. A novel prediction method for down-hole working conditions of the beam pumping unit based on 8-directions chain codes and online sequential extreme learning machine. J. Petrol. Sci. Eng. 160, 285–301. https://doi.org/10.1016/j.petrol.2017.10.052.

Liu, J., Xu, Z., Zhou, L., Nian, Y., Shao, Y., 2019. A statistical feature investigation of the spalling propagation assessment for a ball bearing. MECH MACH THEORY 131, 336–350. https://doi.org/10.1016/j.mechmachtheory.2018.10.007.

Liu, X., Zhou, F., Liu, J., Jiang, L., 2020. Meta-Learning based prototype-relation network for few-shot classification. Neurocomputing 383, 224–234. https://doi.org/10.1016/j.neucom.2019.12.034.

Table 9
Working condition recognition accuracies based on ML-CSNN under different TFS

Dataset	4-way 1-shot				4-way 4-shot			
	1D-TFS	2D-TFS	4D-TFS	8D-TFS	1D-TFS	2D-TFS	4D-TFS	8D-TFS
Dataset A	67.58±3.30	**84.17±2.50**	83.83±2.74	82.83±2.46	74.38±1.71	88.38±1.36	**89.31±1.35**	88.33±1.26
Dataset B	71.17±2.97	83.92±2.56	**87.00±2.34**	86.42±2.29	79.67±1.52	90.77±1.24	**92.83±1.01**	90.58±1.07
Dataset C	75.17 ± 2.61	84.00±2.45	**87.08±2.33**	83.58±2.48	79.44±1.55	89.67±1.31	**92.10±0.96**	90.96±1.04
Dataset D	78.92±2.73	87.17±2.29	**88.92±2.20**	87.92±2.06	84.21±1.32	93.56±0.89	94.08±0.87	**94.10±0.87**

Liu, Z., Cao, H., Chen, X., He, Z., Shen, Z., 2013. Multi-fault classification based on wavelet SVM with PSO algorithm to analyze vibration signals from rolling element bearings. Neurocomputing 99, 399–410. https://doi.org/10.1016/j.neucom.2012.07.019.

Lv, X.-X., Wang, H.-X., Xin, Z., Liu, Y.-X., Zhao, P.-C., 2021a. Adaptive fault diagnosis of sucker rod pump systems based on optimal perceptron and simulation data. Petrol. Sci. https://doi.org/10.1016/j.petsci.2021.09.012.

Lv, X., et al., 2020. A novel method of output metering with dynamometer card for SRPS under fault conditions. J. Petrol. Sci. Eng. 192, 107098. https://doi.org/10.1016/j.petrol.2020.107098, 107098.

Lv, X., et al., 2021b. An evolutional SVM method based on incremental algorithm and simulated indicator diagrams for fault diagnosis in sucker rod pumping systems. J. Petrol. Sci. Eng. 203. https://doi.org/10.1016/j.petrol.2021.108806.

Munkhdalai, T., Yu, H., 2017. Meta networks. In: 34th International Conference on Machine Learning. ICML, pp. 3933–3943. https://doi.org/10.48550/arXiv.1703.00837, 2017.

Peng, Y., 2019. Artificial intelligence applied in sucker rod pumping wells: intelligent dynamometer card generation, diagnosis, and failure detection using deep neural networks. In: Proceedings - SPE Annual Technical Conference and Exhibition. https://doi.org/10.2118/196159-ms.

Pvc, R., Kreidl, M., Sm'Id, R.V., 2005. Condition indicators for gearbox condition monitoring systems. Acta Polytech 45 (6), 58. https://doi.org/10.14311/782.

Ravi, S., Larochelle, H., 2017. Optimization as a model for few-shot learning. In: 5th International Conference on Learning Representations. ICLR 2017. https://openreview.net/pdf?id=rJY0-Kcll.

Ren, Z., et al., 2020. A novel model with the ability of few-shot learning and quick updating for intelligent fault diagnosis. Mech. Syst. Signal Pr. 138. https://doi.org/10.1016/j.ymssp.2019.106608.

Santoro, A., Bartunov, S., Botvinick, M., Wierstra, D., Lillicrap, T., 2016. Meta-learning with memory-augmented neural networks. In: 33rd International Conference on Machine Learning. ICML, pp. 2740–2751, 2016. https://dl.acm.org/doi/10.5555/3045390.3045585.

Sharaf, S.A., 2018. Beam pump dynamometer card prediction using artificial neural networks. KnE Engineering 3 (7). https://doi.org/10.18502/keg.v3i7.3083.

Sun, H., Zheng, X., Lu, X., 2021. A supervised segmentation network for hyperspectral image classification. IEEE T Imag. Proc. 30, 2810–2825. https://doi.org/10.1109/TIP.2021.3055613.

Vinyals, O., Blundell, C., Lillicrap, T., Kavukcuoglu, K., Wierstra, D., 2016. Matching networks for one shot learning. In: 30th Annual Conference on Neural Information Processing Systems. NIPS, pp. 3637–3645. https://doi.org/10.48550/arXiv.1606.04080, 2016.

Wang, W., Shen, J., Shao, L., 2018. Video salient object detection via fully convolutional networks. IEEE T Imag. Proc. 27 (1), 38–49. https://doi.org/10.1109/TIP.2017.2754941.

Wang, X., et al., 2019. A working condition diagnosis model of sucker rod pumping wells based on big data deep learning. In: International Petroleum Technology Conference 2019. https://doi.org/10.2523/iptc-19242-ms. IPTC 2019.

Wu, W., Sun, W.L., Wei, H.X., 2011. A fault diagnosis of suck rod pumping system based on wavelet packet and RBF network. Adv. Mater. Res. 189–193, 2665–2669. https://doi.org/10.4028/www.scientific.net/AMR.189-193.2665.

Wu, Z., Wang, X., Jiang, Y.G., Ye, H., Xue, X., 2015. Modeling spatial-Temporal clues in a hybrid deep learning framework for video classification. In: MM 2015 - Proceedings of the 2015 ACM Multimedia Conference, pp. 461–470. https://doi.org/10.1145/2733373.2806222.

Yan, X., Jia, M., 2018. A novel optimized SVM classification algorithm with multi-domain feature and its application to fault diagnosis of rolling bearing. Neurocomputing 313, 47–64. https://doi.org/10.1016/j.neucom.2018.05.002.

Yu, C., Ning, Y., Qin, Y., Su, W., Zhao, X., 2021. Multi-label fault diagnosis of rolling bearing based on meta-learning. Neural Comput. Appl. 33 (10), 5393–5407. https://doi.org/10.1007/s00521-020-05345-0.

Zhang, A., Gao, X., 2019. Supervised dictionary-based transfer subspace learning and applications for fault diagnosis of sucker rod pumping systems. Neurocomputing 338, 293–306. https://doi.org/10.1016/j.neucom.2019.02.013.

Zhang, J., Su, Q., Liu, P., Gu, H., Wang, W., 2020. A monocular 3D target detection network with perspective projection. Robot 42 (3), 278–288. https://doi.org/10.13973/j.cnki.robot.190221.

Zhang, K., et al., 2022. Fault diagnosis method for sucker rod well with few shots based on meta-transfer learning. J. Petrol. Sci. Eng. 212. https://doi.org/10.1016/j.petrol.2022.110295.

Zhao, H., Wang, J., Gao, P., 2017. A deep learning approach for condition-based monitoring and fault diagnosis of rod pump. Serv. Transac. Internet Thing. 1 (1), 32–42. https://doi.org/10.29268/STIOT.2017.1.1.3.

Zhao, L., Qiu, X., Zhang, Q., Huang, X., 2019. Sequence labeling with deep gated dual path CNN. IEEE-ACM T Audio Spe. 27 (12), 2326–2335. https://doi.org/10.1109/TASLP.2019.2944563.

Zhao, M., Zhong, S., Fu, X., Tang, B., Pecht, M., 2020. Deep residual shrinkage networks for fault diagnosis. IEEE T Ind. Inform. 16 (7), 4681–4690. https://doi.org/10.1109/TII.2019.2943898.

Zheng, B., Gao, X., 2017. Sucker rod pumping diagnosis using valve working position and parameter optimal continuous hidden Markov model. J Process Contr. 59, 1–12. https://doi.org/10.1016/j.jprocont.2017.09.007.

Zheng, B., Gao, X., Li, X., 2019. Fault detection for sucker rod pump based on motor power. Control Eng. Pract. 86, 37–47. https://doi.org/10.1016/j.conengprac.2019.02.001.

Zheng, B., Gao, X., Pan, R., 2020. Sucker rod pump working state diagnosis using motor data and hidden conditional random fields. IEEE T Ind. Electron. 67 (9), 7919–7928. https://doi.org/10.1109/TIE.2019.2944081.

Zhou, W., Li, X., Yi, J., He, H., 2019. A novel UKF-RBF method based on adaptive noise factor for fault diagnosis in pumping unit. IEEE T Ind. Inform. 15 (3), 1415–1424. https://doi.org/10.1109/TII.2018.2839062.